

Design of a High Torque Density Modular Actuator for Dynamic Robots

by

Alexander Hattori

S.B., Massachusetts Institute of Technology (2019)

Submitted to the Department of Mechanical Engineering
in partial fulfillment of the requirements for the degree of

Masters of Science in Mechanical Engineering

at the

MASSACHUSETTS INSTITUTE OF TECHNOLOGY

May 2020

© Massachusetts Institute of Technology 2020. All rights reserved.

Author
Department of Mechanical Engineering
May 15, 2020

Certified by
Sangbae Kim
Professor
Thesis Supervisor

Accepted by
Nicolas Hadjiconstantinou
Professor of Mechanical Engineering
Chairman, Department Committee on Graduate Theses

Design of a High Torque Density Modular Actuator for Dynamic Robots

by

Alexander Hattori

Submitted to the Department of Mechanical Engineering
on May 15, 2020, in partial fulfillment of the
requirements for the degree of
Masters of Science in Mechanical Engineering

Abstract

When designing new control systems for dynamic robots, differences between simulated and real-world physics can cause the robot hardware to experience a significant amount of misuse, often leading to downtime as hardware is continuously repaired and improved. The MIT Biomimetic Robotics Lab aimed to mitigate this problem by building the MIT Mini Cheetah, a low cost, mechanically robust, quadruped that was capable of tolerating the strains of testing new legged robot controls. One of the key design features of the Mini Cheetah that allows it to have minimized repair time compared to other dynamic robots is its use of the same modular actuators at all joints, allowing for easy replacement of components and a simpler mechanical design. These modular actuators consist of a hobby brushless motor with an internal planetary gearbox, a motor controller and a position sensor. This thesis documents the design and manufacturing of the new generation of Mini Cheetah-sized actuators. The new design utilizes a custom rotor design and a new module topology which allow for higher torque density in roughly the same form factor. The new module also incorporates a new, higher resolution encoder allowing for higher torque bandwidth. These new modules will be used in various research projects in the lab including a set of bilaterally teleoperated arms, a humanoid, and a new quadruped.

Thesis Supervisor: Sangbae Kim
Title: Professor

Acknowledgments

The author would like to thank:

Sangbae Kim for being my advisor throughout my time at MIT, from undergrad to grad school, and giving me a place in a lab where I could work on projects that kept me excited and engaged.

Jared DiCarlo for being my best friend and roommate for the last 5 years and teaching me basically everything I know about engineering. Your enthusiasm for controls and robotics is contagious and I'm so glad we got to work on so many projects together over the years.

Ben Katz for taking me under your wing in MITERS and lab and teaching me so much. You inspire me to be a better engineer.

Austin Brown for the late night apartment shenanigans, long productive walks during quarantine, MITERS shenanigans at all hours, and for always fixing my surface mount electronics when I inevitably bridge pins.

Pat McAtamney for being the best shop manager and being my friend. You enabled me to become the machinist I am today and provided me with hundreds of hours of entertainment on the Haas and Waterjet throughout my time at MIT. The table you set up in front of the VF2 became my unoffical desk as a grad student this past year.

Andrew SaLoutos for your advice on designing the module, and your help with finding and implementing the encoders and higher voltage motor controllers.

Zhiyi Liang and John Zhang for being my MechE buddies. I'm looking forward to seeing you both become professors and MIT Lifers some day.

Lili Sun for keeping me company in MITERS, Area 51, ZOOM, and Messenger while I worked on all my various projects.

Harriet Chiu for inspiring me to finish this thesis in a year and for always being willing to listen to me talk about my robots and machining.

Contents

1	Introduction	11
1.1	Motivation	11
1.2	Scope	15
2	Design	17
2.1	Mechanical Design	17
2.2	Motor Constant Selection	25
2.3	Encoder	27
3	Manufacturing	31
3.1	Prototype design	31
3.2	Ring Gear	33
3.3	Stator-Ring Gear Interface	34
3.4	Rotor	42
3.5	Planet Carrier	45
3.6	Small Parts	47
3.7	Outer Housings	49
3.8	Final Manufacturing	52
4	Results	55
4.1	Actuator Specifications	55
4.2	Encoder Data	57
4.3	Finite Element Analysis	67

5 Summary and Conclusions	71
5.1 Design Summary	71

List of Figures

1-1	The original Mini Cheetah actuator design.	12
1-2	The cross section of the original Mini Cheetah actuator design.	13
1-3	The rear bearing section.	14
2-1	A rendering of the final CAD design.	18
2-2	The cross section of the final CAD design.	18
2-3	The exploded cross sectional view of the new actuator.	19
2-4	The locations of the actuators on the original Mini Cheetah robot. . .	20
2-5	Rotor comparison.	21
2-6	Planet carrier comparison.	22
2-7	The roller layout of the crossed roller bearing.	23
2-8	Encoder Layout.	28
2-9	The code carrier topology. [2]	28
3-1	The prototype CAD model.	32
3-2	The ring gear mounted in the Haas CNC Mill before being modified. .	33
3-3	The stator-ring gear interface assembly.	34
3-4	Manufacturing of the ring gear adapter.	35
3-5	The finished ring gear adapter.	35
3-6	The factory wound stator.	36
3-7	An in-progress picture of the stator winding process.	37
3-8	The finished hand wound stator.	38
3-9	The relief angle on the ring gear adapter.	39
3-10	The pressing jig and associated assembly.	40

3-11	The pressing process.	40
3-12	The completed stator assembly.	41
3-13	The CAD rotor assembly.	42
3-14	Probing the smallest possible bore.	43
3-15	The finished rotor assembly.	44
3-16	The completed planet carrier assembly.	45
3-17	The tested gearbox assembly.	46
3-18	The thin washer-like parts.	47
3-19	The wire clip.	48
3-20	The starting billet and fixture plate for the front housing.	49
3-21	The results of the operation to machine the housing front.	49
3-22	Anodized housing assembly.	50
3-23	Completed prototype module.	51
3-24	The front housing.	52
3-25	The rear housing.	53
4-1	Setup for hand drill test.	58
4-2	Old encoder (12-bit) data taken with hand drill test.	59
4-3	New encoder (19-bit) data taken with hand drill test.	60
4-4	Old encoder (12-bit) data taken in constant velocity mode.	61
4-5	New encoder (19-bit) data taken in constant velocity mode.	62
4-6	Old encoder (12-bit) data taken with 0 velocity commanded.	63
4-7	New encoder (19-bit) data taken with 0 velocity commanded.	64
4-8	Old encoder (12-bit) data taken with a step response.	65
4-9	New encoder (19-bit) data taken with a step response.	66
4-10	Bolts for mounting shown in green.	67
4-11	Loading conditions of the actuator output simulated using FEA.	68
4-12	FEA of the module housing under axial loading.	68
4-13	FEA of the module housing under torsional loading.	69

List of Tables

2.1	Description of module components in the exploded cross sectional view.	19
4.1	Motor module parameters	56

Chapter 1

Introduction

1.1 Motivation

In robotics applications, it is highly beneficial to have easily replaceable, self-contained actuators in order to minimize downtime of the robots. For research institutions in particular, where robots are often used for highly dynamic locomotion with untested controllers, durability and ease of repair of the actuators is critical. As a result, the Biomimetic Robotics Lab developed modular robotic actuators used for the Mini Cheetah quadruped and other robotic projects. These actuator modules, developed by Ben Katz and Sangbae Kim, are self-contained motor, gearbox, position sensor, and controller units. The actuator only needs power and a CAN (Controller Area Network) signal and can provide torque, position, and speed control. These were designed to be robust and cost effective so that 10 Mini Cheetah robots could be produced and lent to various research institutions who could benefit from the hardware for developing new controls and software in collaboration with our lab. A CAD model of the completed module is shown in Figure 1-1. These modules cost approximately \$300 per actuator.



Figure 1-1: The original Mini Cheetah actuator design.

These modules work very well, but as our lab starts to develop more advanced, one-off designs, some improvements can be made to the actuator modules. In particular, the motor used in the original Mini Cheetah actuator, an EX-8, is a stock hobby motor. This motor was chosen because of its performance and price; it could be purchased for \$50-\$90 depending on quantity, with a comparable custom motor from T-motor priced on the order of \$300+. As a result of the stock hobby motor geometry, there is some amount of space that is under utilized in the original module, where the rotor of the motor takes up volume, but provides no force. This underutilized space is shown in Figure 1-2. Typical applications of these actuators, where they are linked in tightly packed serial linkages, have the revolved volume of the actuator as a limit rather than simply the volume enclosed by the actuator.

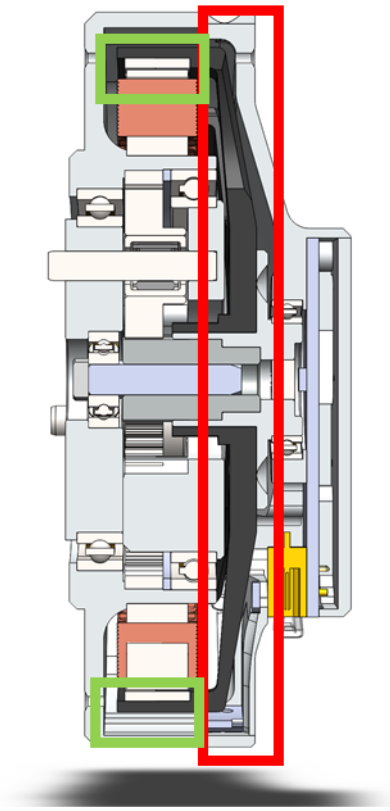


Figure 1-2: The cross section of the original Mini Cheetah actuator design, with the underutilized rotor area boxed in red. The useful length of the rotor magnets is boxed in green.

Additionally, the material added by providing a bearing to support the rotor in the rear part of the housing adds additional width as shown in Figure 1-3.

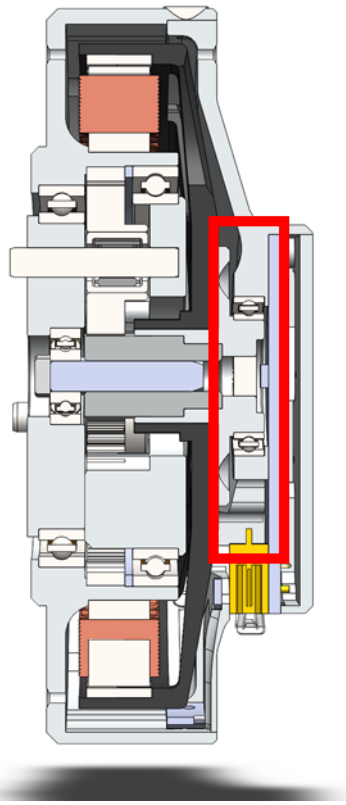


Figure 1-3: The rear bearing section is boxed in red.

Lastly, the actuator used radial bolts to secure the front and back housing pieces together, with no axial constraint besides the countersunk screw heads. This proved to be structural enough, but allowed for slight deviations in overall module thickness, resulting in clearance issues when clamping the module from both sides.

1.2 Scope

This thesis documents the design and manufacturing of a high torque density robotic actuator consisting of a motor, gearbox, position sensor, and motor controller, in one housing. A prototype actuator module was developed in-house and the final design is being produced for use in humanoids, quadrupeds, and bilaterally teleoperated arms. The actuator builds on previous work by Ben Katz and Sangbae Kim who developed the original actuator modules for the Mini Cheetah robot. The new actuator uses a new mechanical topology, an improved mechanical design for the rotor, and a new encoder to improve overall performance while maintaining the same form factor with a small increase in weight.

Chapter 2

Design

2.1 Mechanical Design

This actuator module is designed to be the next generation Mini Cheetah actuator. The iterated design provides improvements and features that our lab learned from using the original actuators. The actuator consists of a large diameter brushless outrunner that houses a planetary gearbox within its stator, and a custom motor controller all integrated into one unit. The actuator receives power and CAN signals, and can be controlled in torque, position, and velocity mode. Additionally, the original actuator was designed to minimize costs as much as possible. This cost restriction was eased for the new module, allowing for a custom mechanical motor design, unlike the use of a post machined stock motor used in the original actuator.

A noted problem on the previous design is the lack of axial retention for the front and back pieces of the outer housing, which resulted in slight variations in thickness from module to module. The change from radial to axial housing bolts drives the diameter increase in the new module.

Figure 2-1 shows the new actuator CAD model and Figure 2-2 shows the cross section. The new design has roughly the same overall form factor as the original module, but with twice as much motor volume.



Figure 2-1: A rendering of the final CAD design.

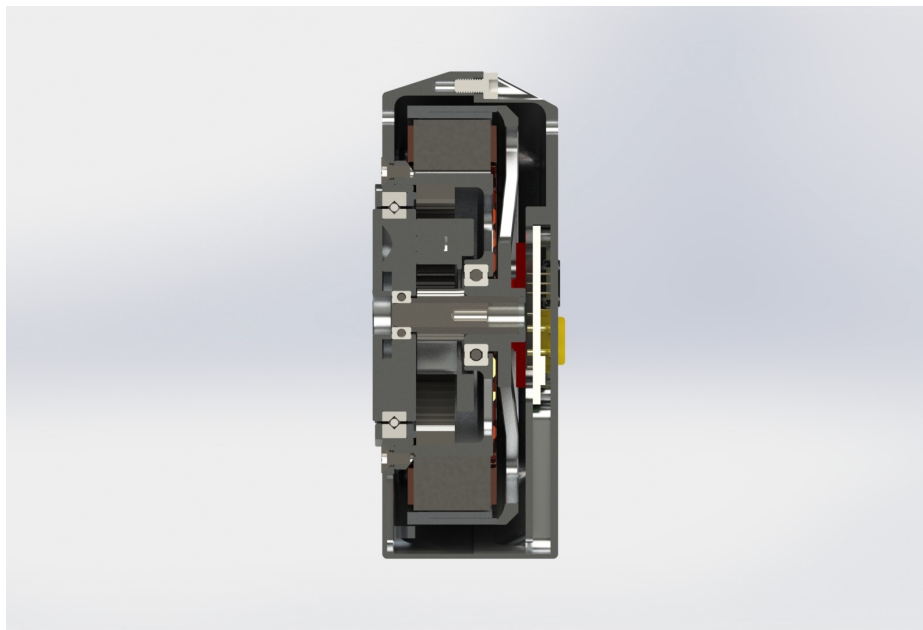


Figure 2-2: The cross section of the final CAD design.

Figure 2-3 shows an exploded cross sectional view of the new actuator design. Table 2.1 describes the labels in Figure 2-3.

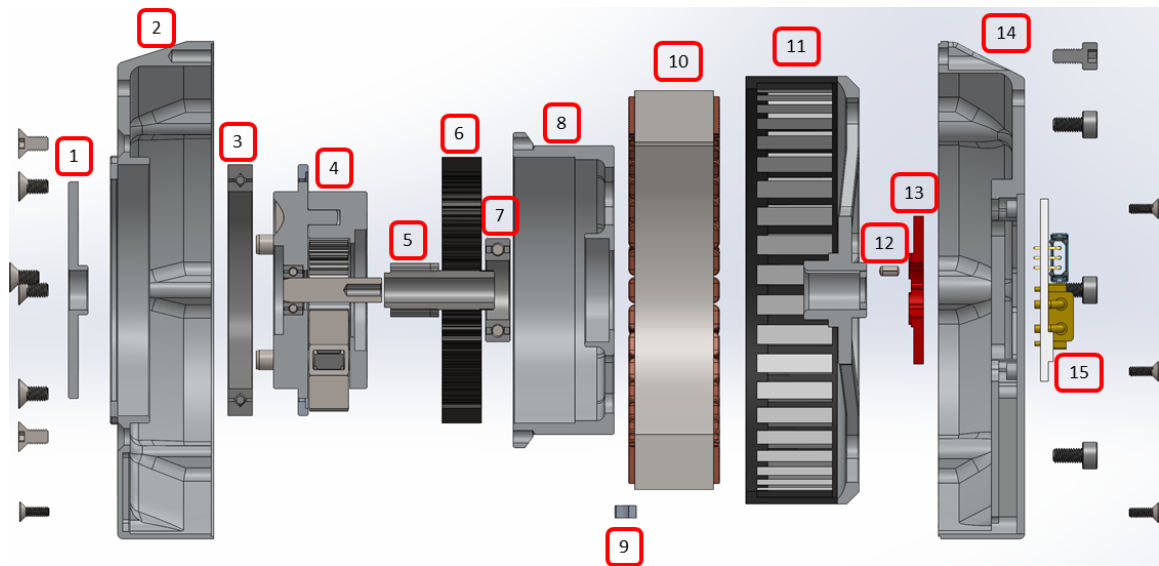


Figure 2-3: The exploded cross sectional view of the new actuator.

Label Number	Purpose
1	Clamping washer which locks the planet carrier to the crossed roller bearing
2	Front housing
3	Crossed roller bearing
4	Planet carrier assembly - Contains the front support bearing for the rotor
5	Pinion gear
6	Ring gear
7	Rotor rear support bearing
8	Ring gear adapter
9	Wire clip
10	Stator
11	Rotor
12	Pin to transmit torque from the rotor to the pinion
13	Magnetic code carrier for encoder
14	Rear housing
15	Motor controller

Table 2.1: Description of module components in the exploded cross sectional view.

This actuator and the previous Mini Cheetah actuator were designed to have the driven load mounted directly on their outputs, allowing for a very compact, simple, and robust serial linkage implementation as shown in the original Mini Cheetah CAD model shown in Figure 2-4. In order to minimize collisions of the actuators with one another and keep overall form factor to a minimum (which increases stiffness and decreases moment of inertia among other benefits), the overall rotational volume consumed by the module is important to consider. This was a key driving factor in the mechanical design.

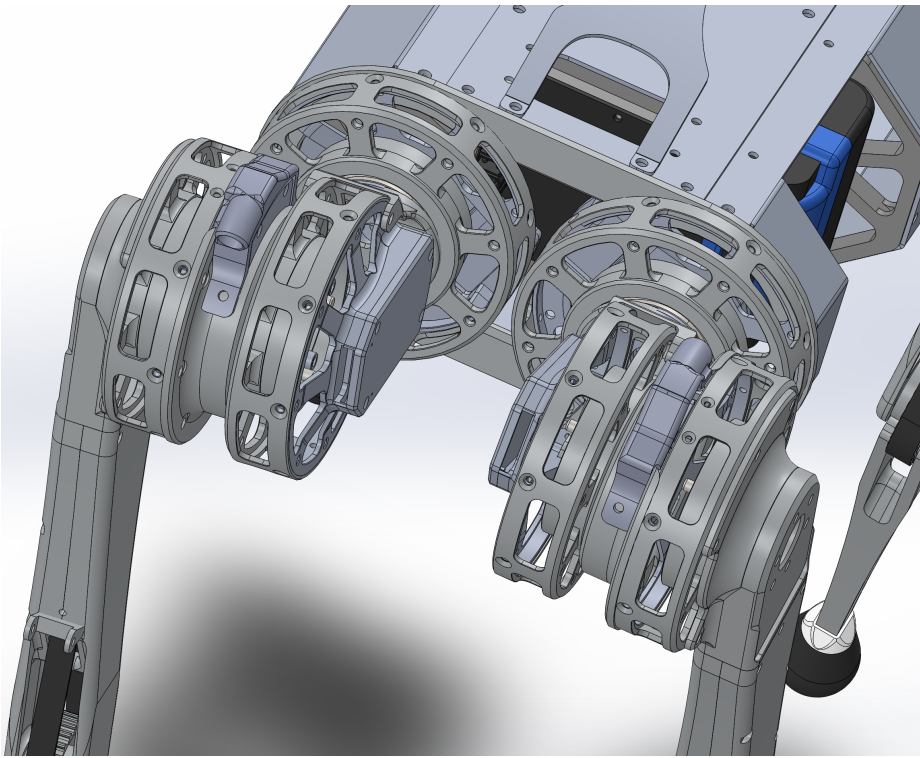


Figure 2-4: The locations of the actuators on the original Mini Cheetah robot.

In order to keep the new module design small, the internal components were first redesigned to be more compact and space efficient. One of the inefficient uses of space in the original actuator was the use of the stock motor rotor. The motor has a significant structural portion which causes the rotor to be longer but does not contain any magnets and thus does not produce torque. The new module utilizes a custom mechanical rotor design that allows for twice the magnet length, in the same module form factor, while maintaining enough structural integrity for the design. While the

previous design used a motor that was comparable to the U8 from T-motor, the new design can now use a U10 motor for the base design. (Note: the U10 II is not comparable to the U10 used.) The comparison of rotors is shown in Figure 2-5.

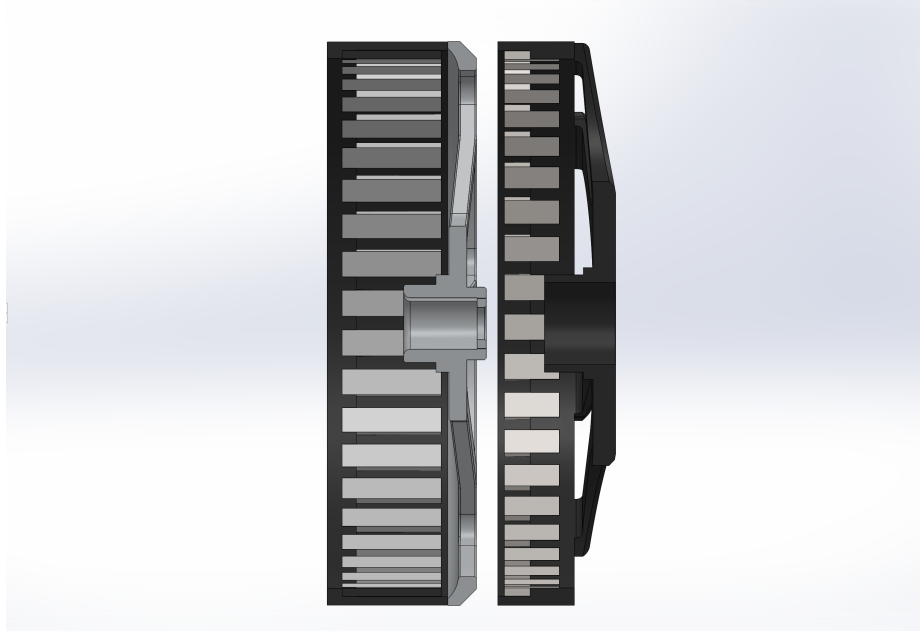


Figure 2-5: The new rotor design shown on the left has double the length of magnet of the previous rotor, but similar encompassed volume.

As a result of utilizing a rotor twice the length of that of the previous design, the module uses an appropriately sized stator (double the length), resulting in a peak torque twice that of the previous design. The gear module was increased from 0.5 mod to 0.8 mod to account for the increased torque on the pinion, and the planetary gears are now the full width of the module. The comparison of the cross sections of the two gearbox assemblies is shown in Figure 2-6.

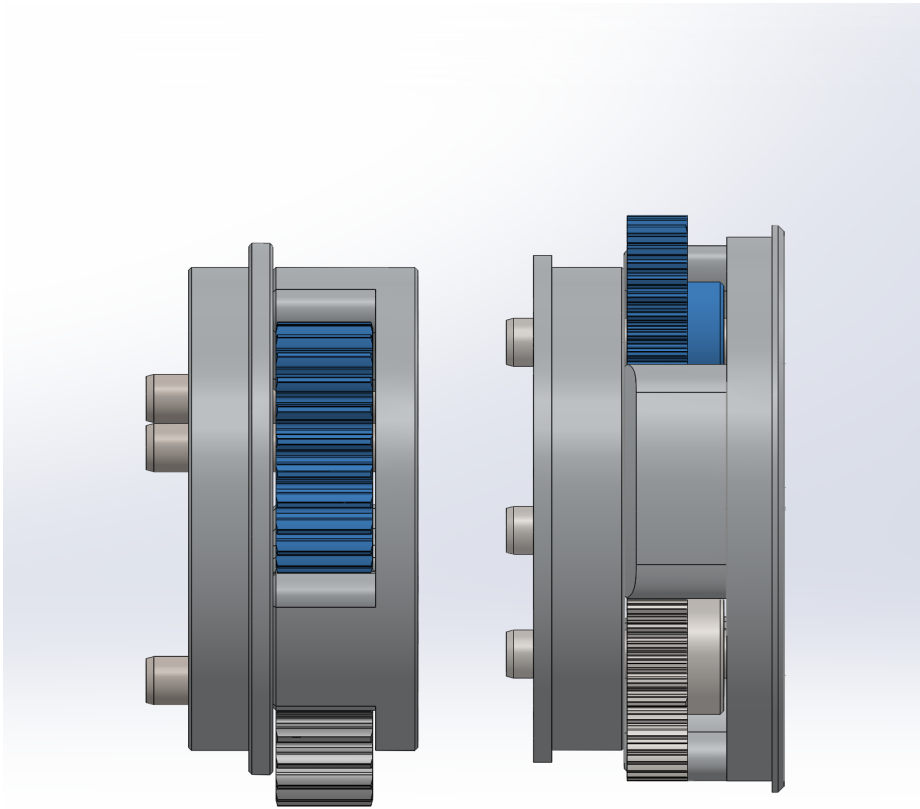


Figure 2-6: The new planet gear assembly, shown on the left, compared to the original planet gear assembly on the right.

The last significant design improvement was the use of a crossed roller bearing to support the output of the module. The roller layout of the IKOCRBT405A bearing used in this design is shown in Figure 2-7. This single crossed roller bearing mounted at the output of the module (considered the front of the module) can support a significantly higher load compared to the two ball bearings used at either end of the previous module. Additionally, due to the nature of the bearing design, the bearing is much stiffer in axial, radial, and torsional loading. The downsides recognized from using this type of bearing in the new design include a small increase in friction/damping, as well as a significant cost increase (\$100 for one crossed roller bearing compared to <\$3 for a ball bearing).



Figure 2-7: The roller layout of the crossed roller bearing.

A new type of magnetic encoder was also used for the new design, with more details provided in the Encoder section.

2.2 Motor Constant Selection

Selection of a motor torque constant for an actuator can often be tricky, especially when designing a single actuator for many different possible use cases. In this design, the actuator has use cases in bilaterally teleoperated arms, humanoid arms and legs, and quadruped legs. As a result, the list of possible constraints is rather large. Fortunately, the applications will be designed around the actuators which in turn, relaxes constraints on the actuator itself. The tradeoff for choosing the motor constant is related to maximum torque, maximum speed, and limitations from the motor driver. This actuator uses the same motor controller designed for the previous Mini Cheetah actuators, with only a slight modification of using components with higher voltage ratings on the power stage. As a result, many of the limitations from the original actuator design are the same. This section focuses on choosing the speed constant of the motor, KV, which can then be used to compute the torque constant, KT.

The peak torque of the motor occurs when the stator is saturated which is based on the geometry of the stator. Torque produced by the motor is proportional to current until the saturation torque is reached. It's important to note that the motor has a saturation torque, but not directly a saturation current. In general, the torque saturation scales with stator or rotor surface area which should be the same but sometimes one is easier to measure than the other. In the case of this module design, the stator is the same as the previous Mini Cheetah actuator, but twice as thick, resulting in a theoretical peak torque of 34 N·m whereas the previous actuators could produce up to 17 N·m [3]. Doubling the stator thickness is analogous to putting two of the same motors on the same shaft, which would provide double the torque of just one motor.

The first design constraint considered was the ability to achieve max torque with the given motor controller. The original actuator achieved its peak torque of 17 N*m [3] with a current of around 30 A. The motor controller can only produce up to 40A for a limited amount of time, so using the same motor KV (105 rpm/V) as the original actuator would not allow the new actuator to achieve double the torque. Lowering the

KV increases the torque constant, meaning that actuator will reach its peak torque at a lower current. However, this means that the motor will have a lower top speed for a fixed voltage.

Conveniently, this actuator will be used with double the voltage of the original actuator, so even if the KV is halved, the module will still have the same top speed as the previous actuator, while having twice the torque constant. As a result, a KV of 50 was chosen, compared to the 105 KV used in the previous actuator. If an application requires peak torque for a longer period of time but can sacrifice top speed, a lower motor KV can be chosen which would allow the motor to reach its saturation torque at a lower current, thus easing the thermal load on the motor controller.

The prototype module used a stock KV motor (100 KV) and is different from the final design.

2.3 Encoder

One of the improvements to the electronics of the module was the use of a magnetic off-axis encoder integrated circuit (IC) made by iC Haus. This uses a 32-pole pair magnet (the magnetic code carrier), attached to the motor rotor, and an IC on the motor controller to determine the absolute position of the rotor with 19 bits of position resolution for one rotation of the motor [1]. This replaces the diametric magnet setup which was good for 12 bits of position resolution used in the previous module. The encoder is used for the field oriented control (FOC) used to drive the motor. Besides higher resolution position data, this encoder also has a hollow center which is useful for applications involving a hollow center module including passing wiring for additional modules through on a serial actuator design. However, this feature was not needed for the applications this module was designed for. The physical locations of the encoder components are shown in Figure 2-8, and the topology of the code carrier is shown in Figure 2-9.

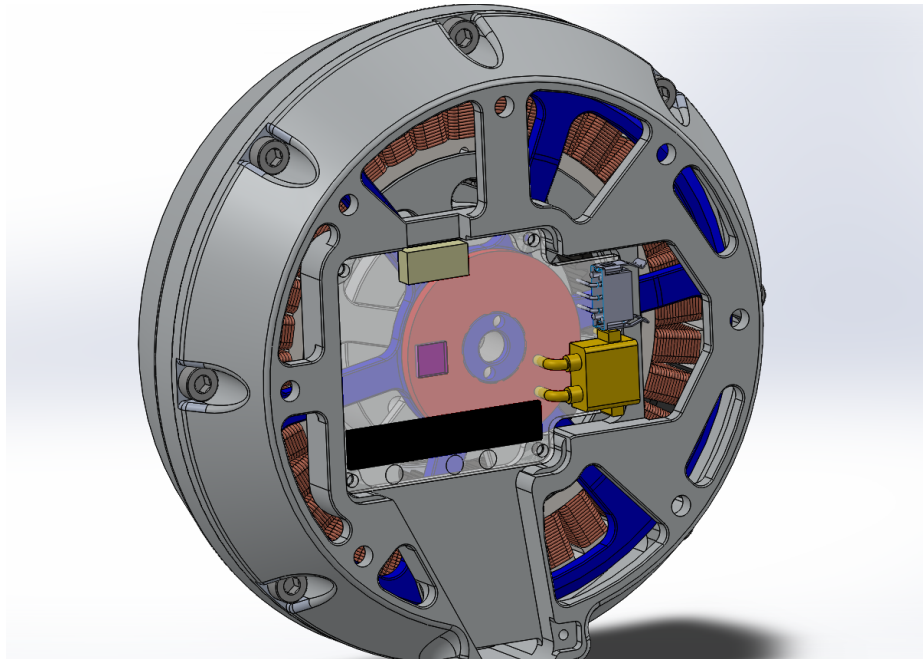


Figure 2-8: Encoder Layout. The rotor is highlighted in blue, the encoder magnet in red, and the encoder IC on the PCB in pink.

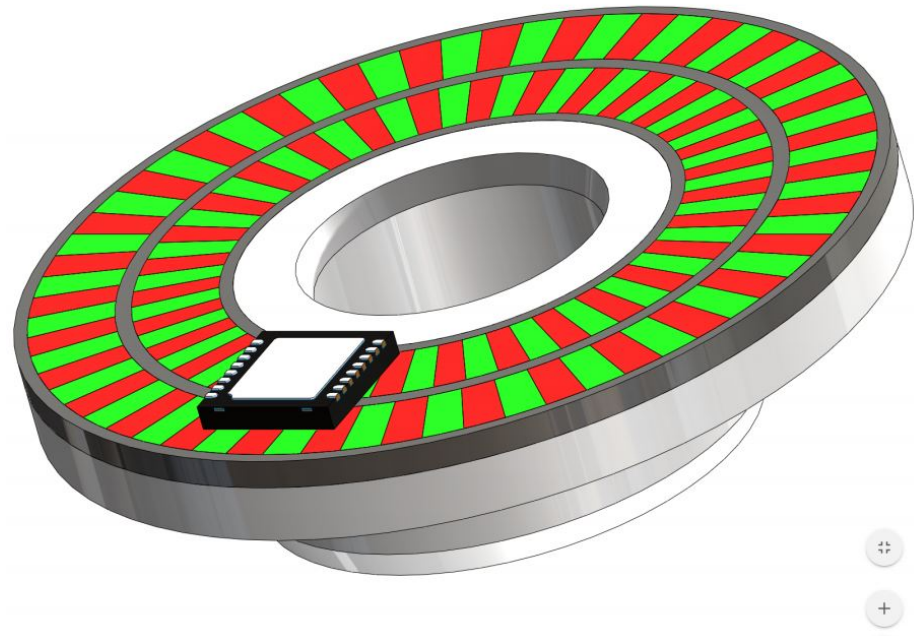


Figure 2-9: The code carrier topology. [2]

There are a few different magnetic code carriers that can be utilized with the same IC, depending on form factor and max rotational speed. The particular 32-pole pair carrier used in this module is capable of measuring position at speeds of up to 12000 rpm which is significantly higher than the rotor speed any variation of this module will see and was chosen due to its availability.

Due to the topology of this module, in particular, the use of a single crossed roller bearing at the output, the position of the encoder IC and the magnetic code carrier relative to each other is highly dependent on the stiffness of the housing when the output is loaded. As a result, FEA was used to find the max displacement of the encoder magnet and IC to make sure they fell within the permissible radial and axial displacements from nominal, found in the datasheet. Some of the FEA simulations are described in the FEA section.

Chapter 3

Manufacturing

3.1 Prototype design

A prototype of the actuator module was made in-house in order to verify the design integrity before sending out for a production run. This section documents a few of the difficult parts to manufacture and assemble. The CAD model for the manufactured prototype is shown in Figure 3-1.

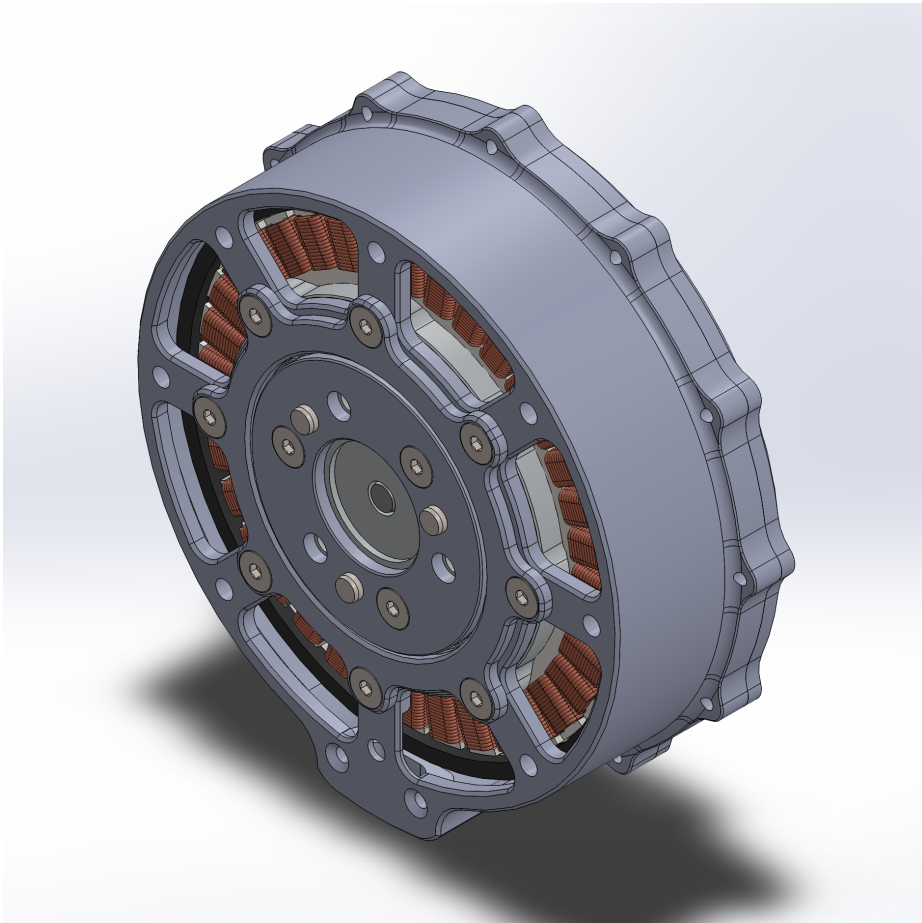


Figure 3-1: The prototype CAD model.

3.2 Ring Gear

The ring gear was a modified KHK 0.8 mod ring gear. It was clamped with an arbor on a custom jig plate and the outer diameter was modified. The ring gear in the fixture is shown in Figure 3-2.

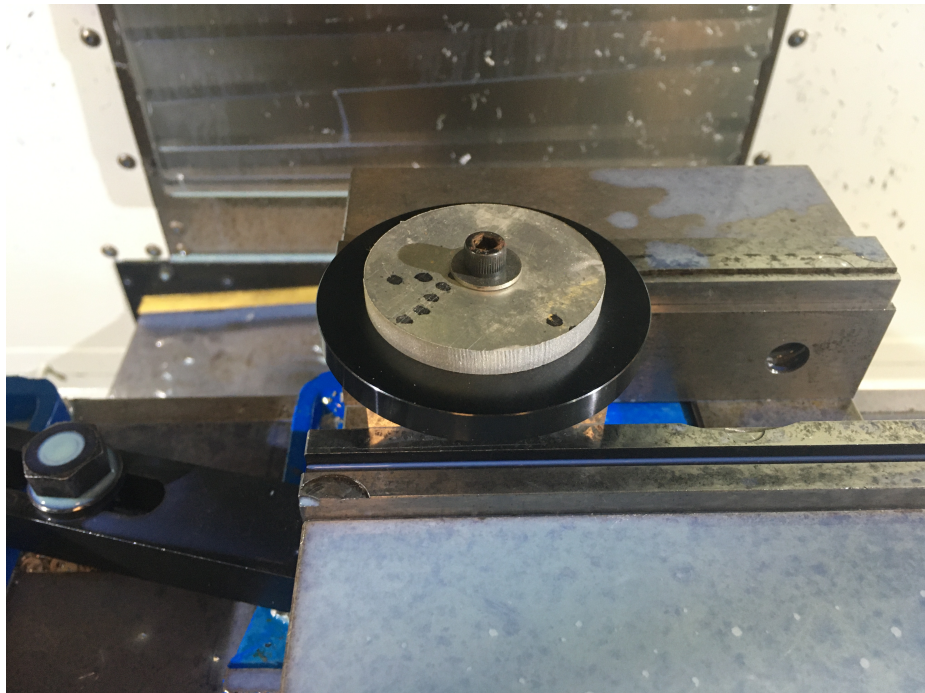


Figure 3-2: The ring gear mounted in the Haas CNC Mill before being modified.

3.3 Stator-Ring Gear Interface

The most difficult assembly to manufacture was the aluminum piece that is pressed into the stator, with the assembly shown in Figure 3-3. The machined aluminum piece, known as the ring gear adapter, is pressed into the stator, while both the ring gear and a bearing to support the rotor are pressed into the aluminum piece. Additionally, the front housing piece, which contains the crossed roller bearing, locates off the same bore as the ring gear. As a result, this piece is the core piece of the module off of which all the other simpler assemblies locate.

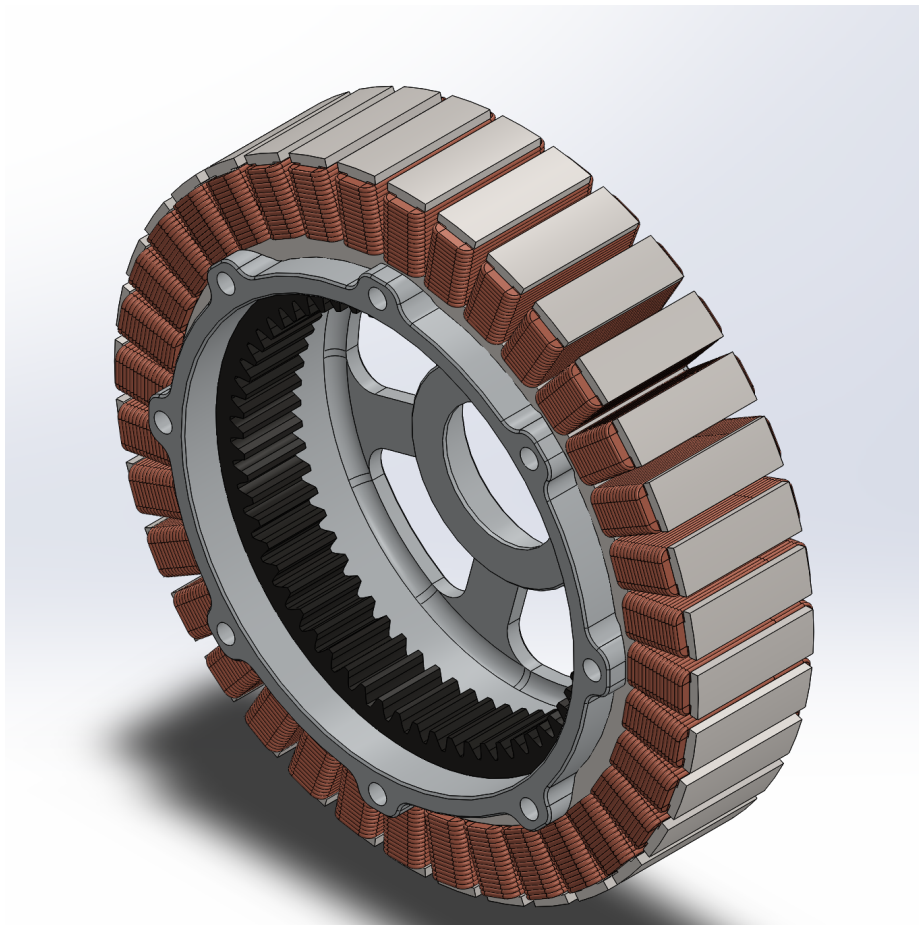
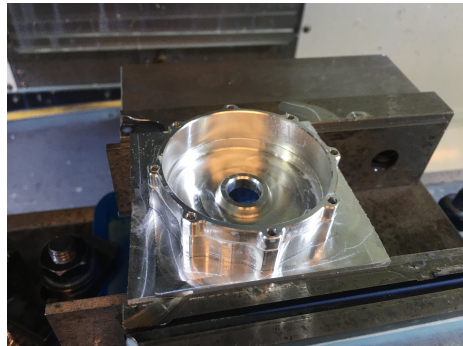


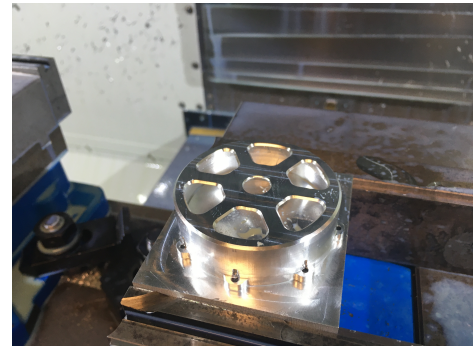
Figure 3-3: The stator-ring gear interface assembly.

The CNC machining of the ring gear adapter was not difficult. The majority of the material was removed in one operation, then the part was flipped over and held by a jig plate and finished. The machining fixtures are shown in Figure 3-4. The

finished part is shown in Figure 3-5.



(a) The first machining operation.



(b) The second machining operation.

Figure 3-4: Manufacturing of the ring gear adapter. Note that the second operation picture was from an earlier iteration so the bearing pocket is different.



Figure 3-5: The finished ring gear adapter.

The difficulty regarding this piece came with the assembly process. The windings

on the stator are not as compact or organized as the CAD model suggests. The linking wire between the windings on individual stator teeth proved to be problematic. The factory wound stator is shown in Figure 3-6.



Figure 3-6: The factory wound stator.

The stator is wound in such a way that an object can easily be pressed through the center without damaging the windings. However, this design utilizes the flower petal bolt pattern which protrudes into some of the territory that the windings occupy. There can be significant electrical noise problems if a single phase of the motor is shorted to the module housing, and obvious electrical shorting problems if multiple phases are shorted and so the difficulty came from ensuring no windings were damaged when pressing in the aluminum ring gear adapter. The first stator assembled had a single strand of winding crushed by one of the flower petals when being pressed and so that stator was no longer usable.

A different assembly method of pressing in the aluminum piece into an unwound stator and then rewinding the stator was attempted, but the windings were not as compact as the factory-wound stator, so that stator was not used. It was a successful stator in the sense that all three phase resistances were the same and there were no

shorts between any phases and the frame. Some of the hand winding process is shown in Figure 3-7 and the final hand wound stator is shown in Figure 3-8.

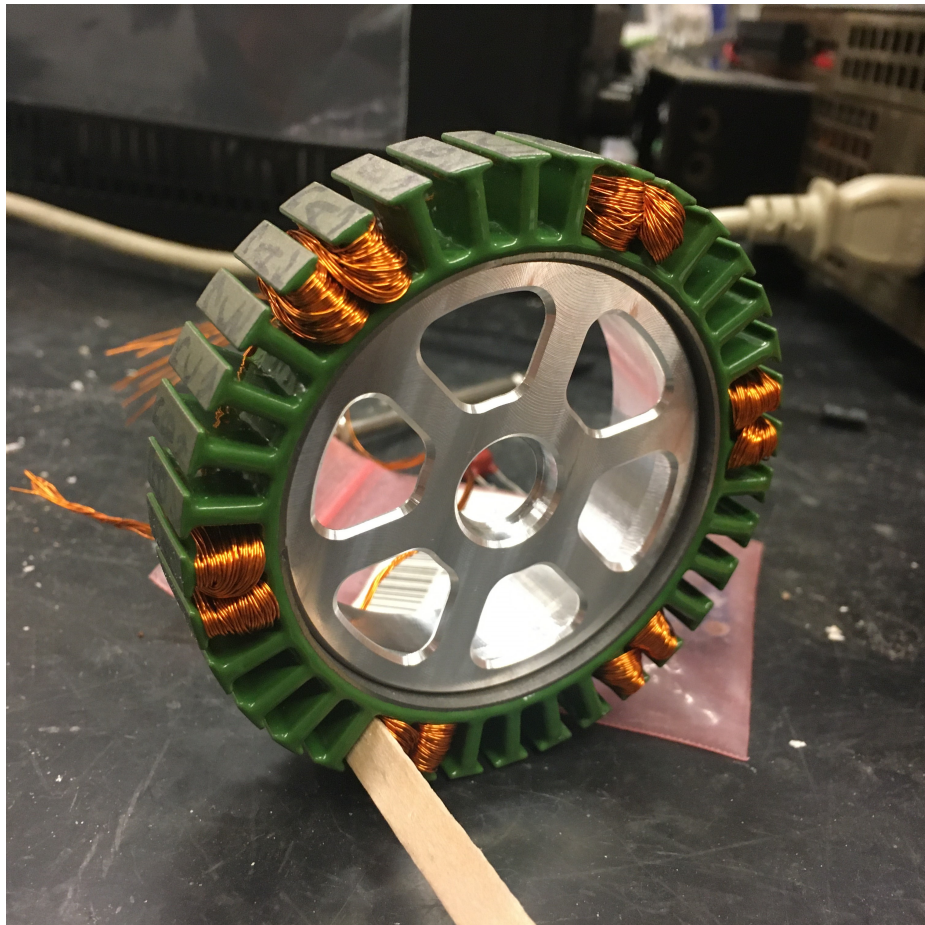


Figure 3-7: An in-progress picture of the stator winding process.



Figure 3-8: The finished hand wound stator.

The assembly method used for the prototype module involved modifying the ring gear adapter (without losing the structural integrity of the threads) to include a relief angle for the windings, insulating the ring gear adapter petals with nail polish, and machining a custom pressing jig. The relief angle is shown in Figure 3-9.

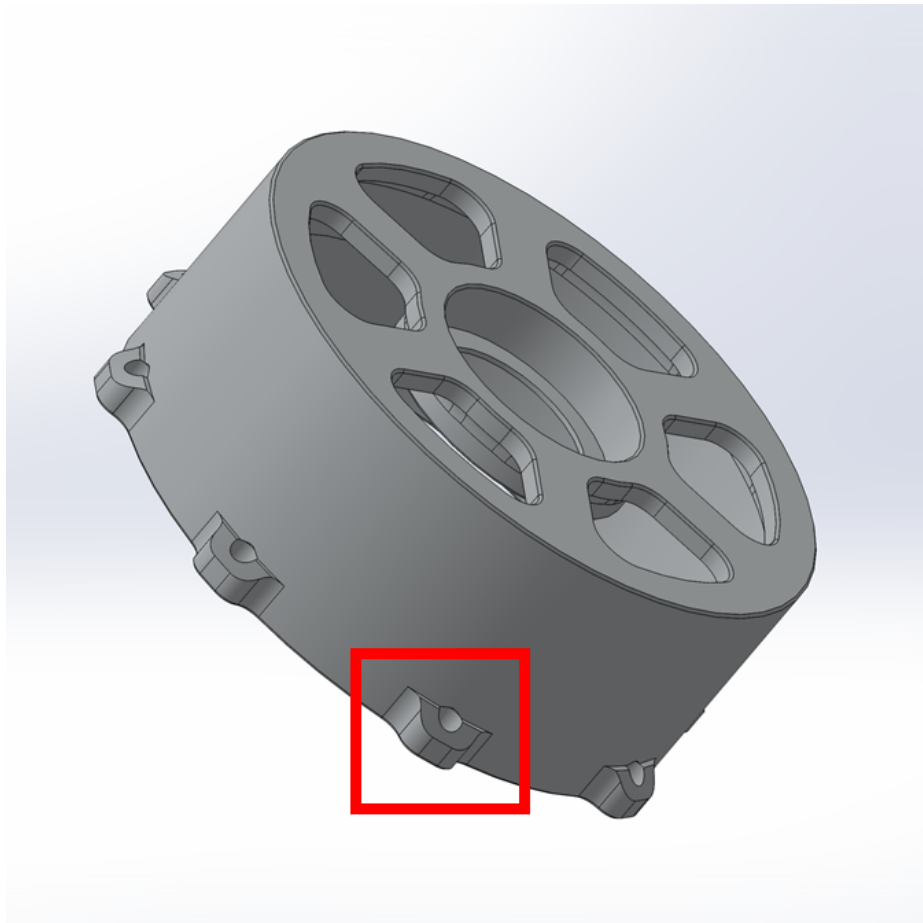
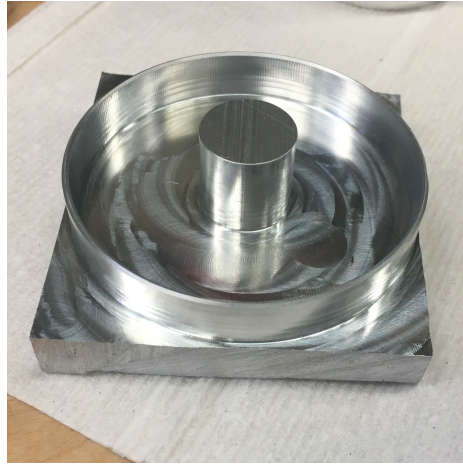
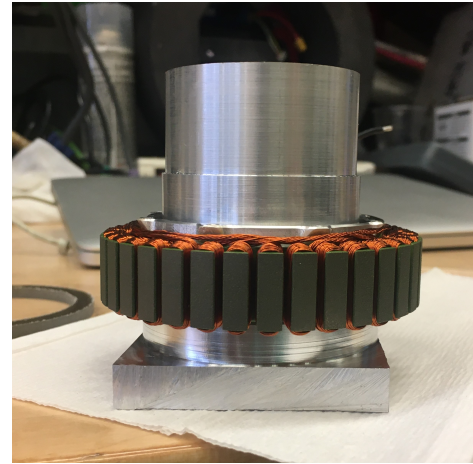


Figure 3-9: The relief angle on the ring gear adapter.

The pressing jig has a thin edge to hold the stator in place without the risk of damaging the windings and a locating boss that fits into the bearing bore on the ring gear adapter. The pressing jig and the pressed assembly are shown in Figure 3-10.



(a) The pressing jig.



(b) The pressing jig assembly.

Figure 3-10: The pressing jig and associated assembly.

The process of pressing the ring gear adapter into the stator, shown in Figure 3-11, was painless for a single stator, but this prototype proved that it would be extremely beneficial to have the company that manufactured the stator to manufacture and assemble the ring gear adapter as well.



Figure 3-11: The pressing process.

The final stator assembly is shown in Figure 3-12.

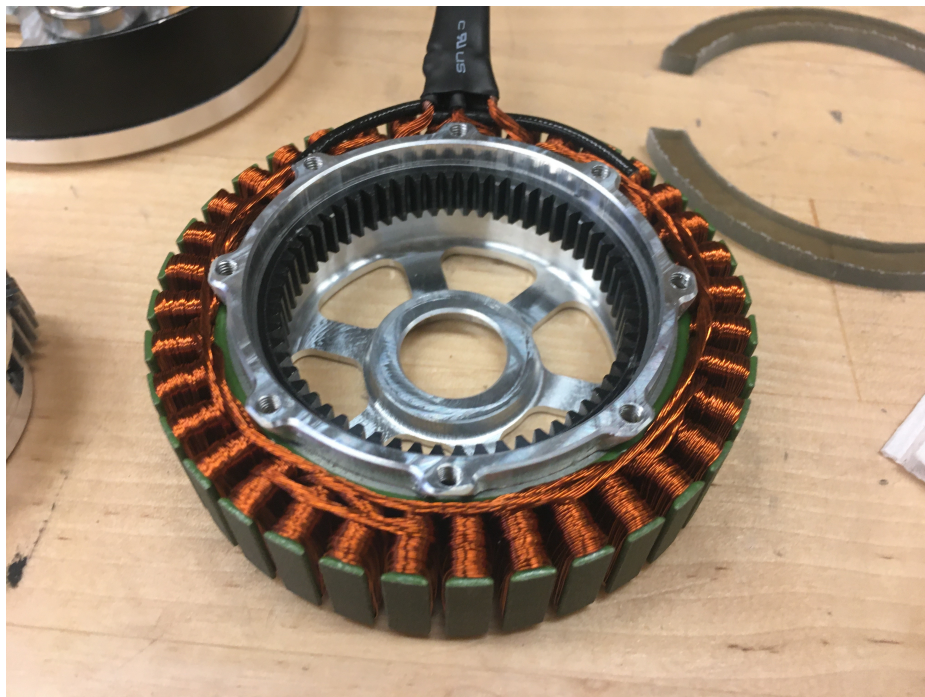


Figure 3-12: The completed stator assembly.

3.4 Rotor

The rotor assembly consists of the rotor magnet ring, an aluminum structural piece (rotor end piece), and the pinion. Additionally, the encoder magnet is pressed onto the rotor end piece, which fits through a bearing in the ring gear adapter assembly. The CAD assembly is shown in Figure 3-13.

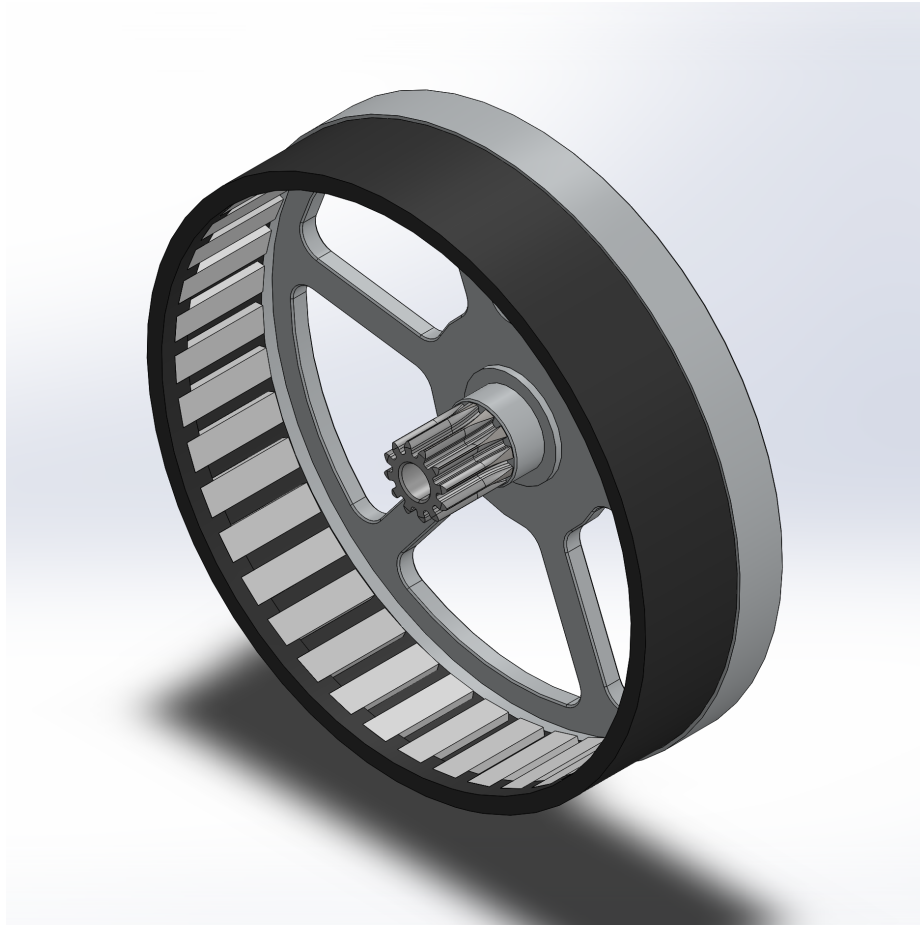
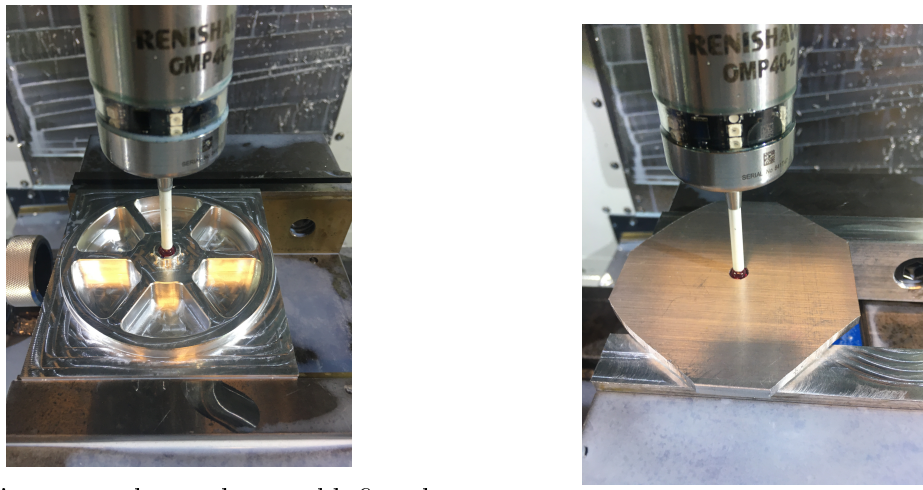


Figure 3-13: The CAD rotor assembly.

In normal production, the rotor end piece and the rotor magnet ring are a single unit (usually a bolted connection, but each manufacturer has its own method) made by the motor manufacturer, but due to the one-off nature of the prototype, the rotor was two pieces press fit together. The small increase in diameter on the rotor (.25 mm) is negligible for clearance within the module.

Machining the rotor was straightforward, with most of the material removed in

one operation, followed by a flip into soft jaws, and finishing of the part. The 1 mm radii needed for the encoder magnet ring locating features were done by drilling holes before the material was machined. The bore in the center of the part was at the limit of the smallest internal diameter the Renishaw probe on the Haas could indicate, as shown in Figure 3-14. Although it was not needed in this situation, an alternative for picking up a very small bore with the probe is to press a pin into the bore, and indicate off the OD of the pin instead.



(a) Making sure the probe would fit when flipped over.
(b) It does indeed fit.

Figure 3-14: Probing the smallest possible bore.

The pinion was machined from a stock Misumi gear which was held in soft jaws. The pinion and the rotor were both aggressively chamfered so that when the steel pinion was pressed into the aluminum rotor end piece, the aluminum part did not form a chip and make the pinion eccentric. The assembled rotor is shown in Figure 3-15.



Figure 3-15: The finished rotor assembly.

3.5 Planet Carrier

The planet carrier was virtually unchanged between the previous Mini Cheetah actuator and this one. The bolt pattern is different to allow for more bolts for the washer plate which clamps the carrier to the crossed roller bearing. Each planet gear is supported across its whole length with a needle roller bearing, and the gears are shimmed to reduce slop and keep friction low without the use of a thrust or ball bearing. The completed planet carrier is shown in Figure 3-16.



Figure 3-16: The completed planet carrier assembly.

Additionally, the gearbox assembly was tested by nesting the appropriate components before they were all pressed and bolted in place. This is shown in Figure 3-17.



Figure 3-17: The tested gearbox assembly.

3.6 Small Parts

There are a few washer-like plates that are designed to be 2 mm thick. They were made by first waterjetting 1/8" thick blanks with the rough geometry. Then they were bolted to a jig plate to finish the outer and inner contours. Lastly, they were countersunk to the proper depth as if they were 2 mm thick, then they were bolted to a fixture and turned to thickness. The final parts are shown in Figure 3-18.



Figure 3-18: The thin washer-like parts.

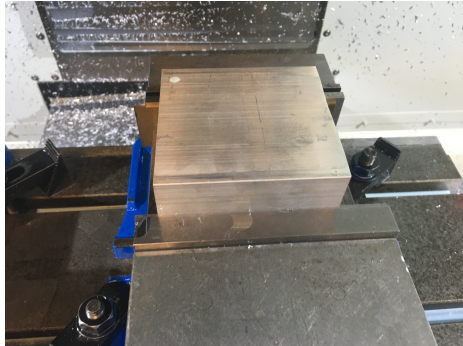
The wire clip, shown in Figure 3-19, was made by waterjetting a blank and drilling and tapping the mounting holes on a mill afterwards.



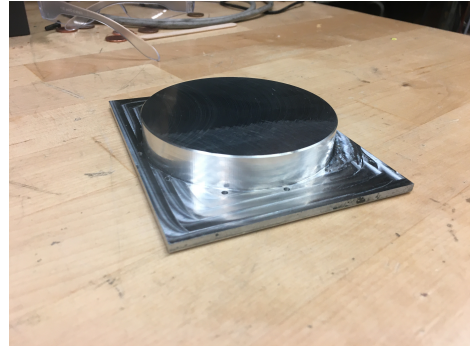
Figure 3-19: The wire clip.

3.7 Outer Housings

The main outer housing piece started off as a large billet and had almost 95% of its material removed by weight. It was made using the usual method of machining most of the material in the first operation, and bolting it to a fixture plate to finish it. The operations are shown in the following figures.



(a) The starting billet for the housing.

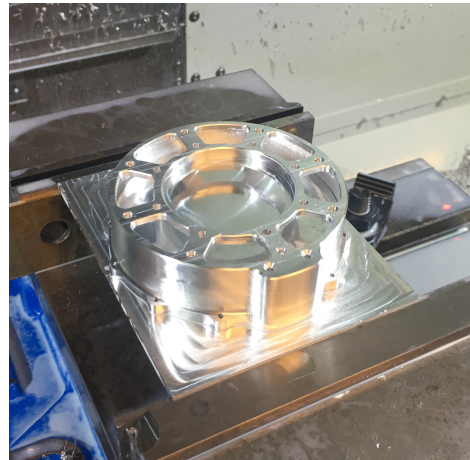


(b) The fixture plate for the second operation.

Figure 3-20: The starting billet and fixture plate for the front housing.



(a) The result of the first operation.



(b) The result of the second operation.

Figure 3-21: The results of the operation to machine the housing front.

Additionally, an unused earlier housing was anodized which is shown in Figure 3-22.

Figure 3-23 shows the completed prototype module in its housing.

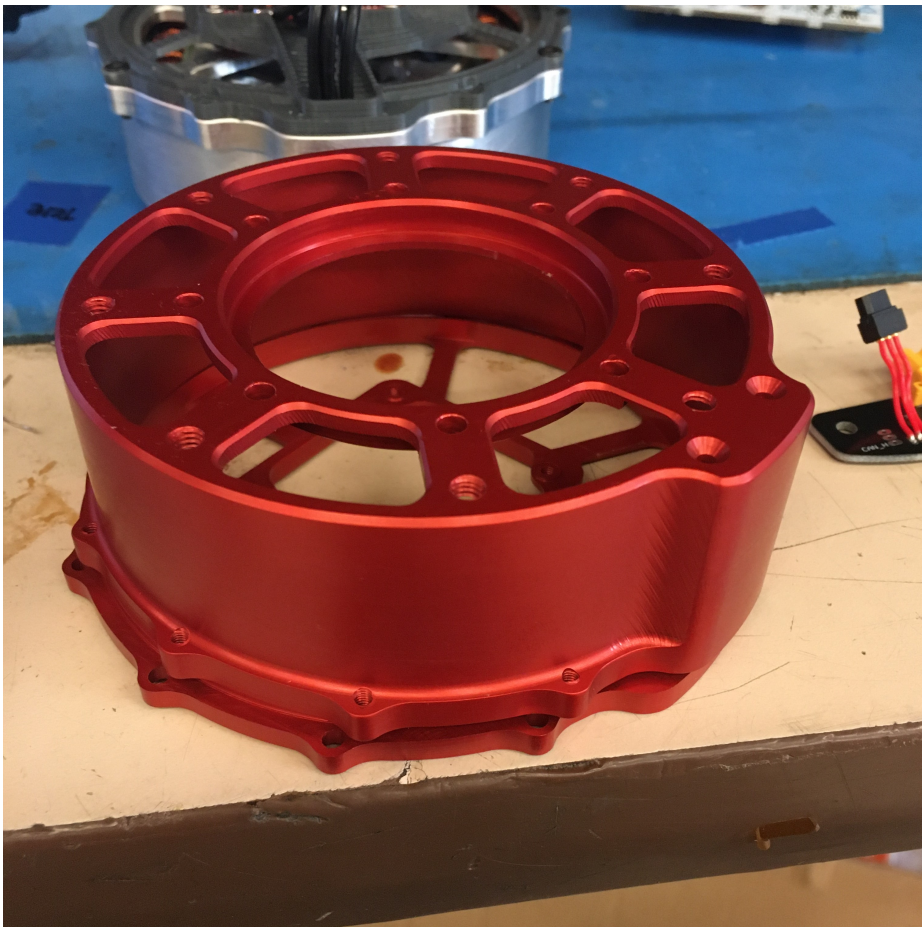


Figure 3-22: Anodized housing assembly.



Figure 3-23: Completed prototype module.

3.8 Final Manufacturing

The main change to the design between the prototype and the production version was to the outer housing. The flanged design where the housing bolts were located towards the rear of the module was changed to a tapered design with the bolts located in the center of the module. The bolt placement was changed to minimize the volume swept when revolving the module, because it was designed to be used in serial linkages in close proximity to each other. The addition of the sloping edge is so in the event of a collision of the actuator with another object, the object is more likely to ride along the edge rather than catching a flat face and damaging the module. The final housing piece designs are shown in Figure 3-24 and Figure 3-25.



Figure 3-24: The front housing.

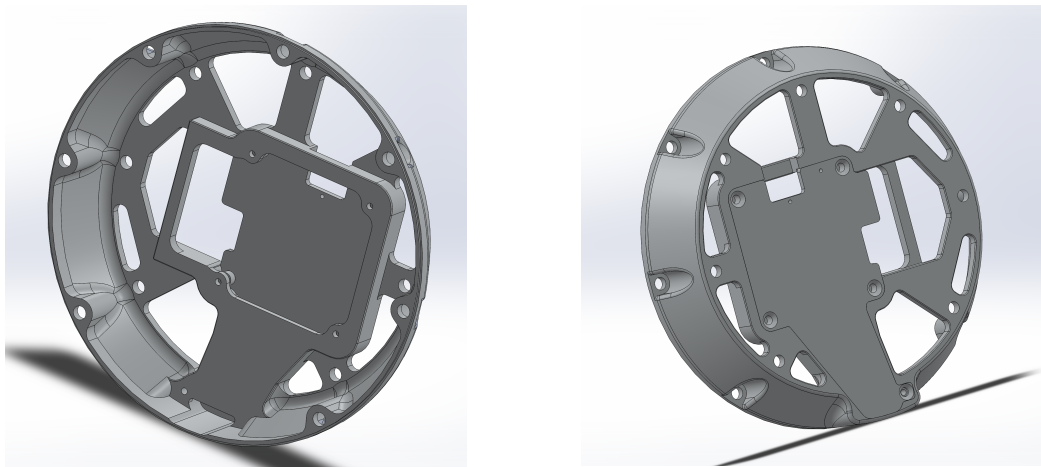


Figure 3-25: The rear housing.

The actuators cost around \$650 a piece, without electronics, so the cost increase seen by using a custom motor and crossed roller bearing is minimal for the smaller quantity of these modules produced compared to the previous Mini Cheetah actuators.

Chapter 4

Results

4.1 Actuator Specifications

Table 4.1 shows the theoretical actuator module parameters. Physical parameters like mass, diameter, and width were estimated from the CAD model, while physical motor parameters like torque and speed are approximated from test data from the original actuator modules. The KV (defined in rpm/V), was given to the motor manufacturer to achieve the proper windings. Saturation torque is approximated from the fact that the stator is twice as thick, resulting in twice the volume of stator to saturate. Continuous torque is approximated from the assumption that the same controller can dissipate the same amount of power.

Parameter	New Module	Mini Cheetah Module
Mass	630 g	480 g
Diameter (peak)	101 mm	96 mm
Width (peak)	38.5 mm	37.3 mm
KV	50 rpm/V	105 rpm/V
KT	.19 N·m/A	.09 N·m/A
Gear Ratio	6:1	6:1
Saturation Torque	34 N·m	17 N·m
Current at Torque Saturation	~30 A	~31 A
Continuous Torque	14.5 N·m	6.9 N·m
Continuous Current	12.6 A	12.6 A
Free Speed	~42 rad/s @ 48V	~40 rad/s @ 24V
Torque Density	54 N·m/kg	35 N·m/kg

Table 4.1: Motor module parameters

4.2 Encoder Data

The desire for a higher resolution encoder stems from our lab's use of these motor modules for bilaterally teleoperated setups. The limitation on stiffness of our lab's bilaterally teleoperated arms is dictated by stability of the controller. Each arm uses a PD controller to try to match its position to the position of the other arm. With high gains, the position encoder noise can be amplified and cause instability. These higher resolution encoders, however, can allow for more stiffness of the arms as long as noise is reduced.

In order to test the improvement in encoder noise as a result of increased resolution, the relevant position and velocity data were sent from the motor controller to a Nucleo F446 microcontroller over CAN, and then recorded in MATLAB over serial. Position data is acquired by the motor controller over SPI directly from the encoder IC, and the position data is differentiated at 40 kHz onboard. The 12-bit encoder data was taken on the previous Mini Cheetah actuator and the 19-bit encoder data was taken on the prototype module. Both modules utilize the same torque constant motor and gear ratio, but have different drag and inertias. However, for this application, we care about overall module performance and so the comparison was still useful.

The first tests were done with the motor controllers disabled to mitigate any possible noise from motor control loop instability or driving characteristics. In order to provide a velocity to the encoder, hex adapters were made so the output of the two modules could be driven by a hand drill at a relatively constant velocity. The adapters and setup are shown in Figure 4-1.



(a) The hex adapter on the prototype module.



(b) The hand drill test setup.

Figure 4-1: Setup for hand drill test.

The data from this hand drill test is shown in Figure 4-2 and Figure 4-3.

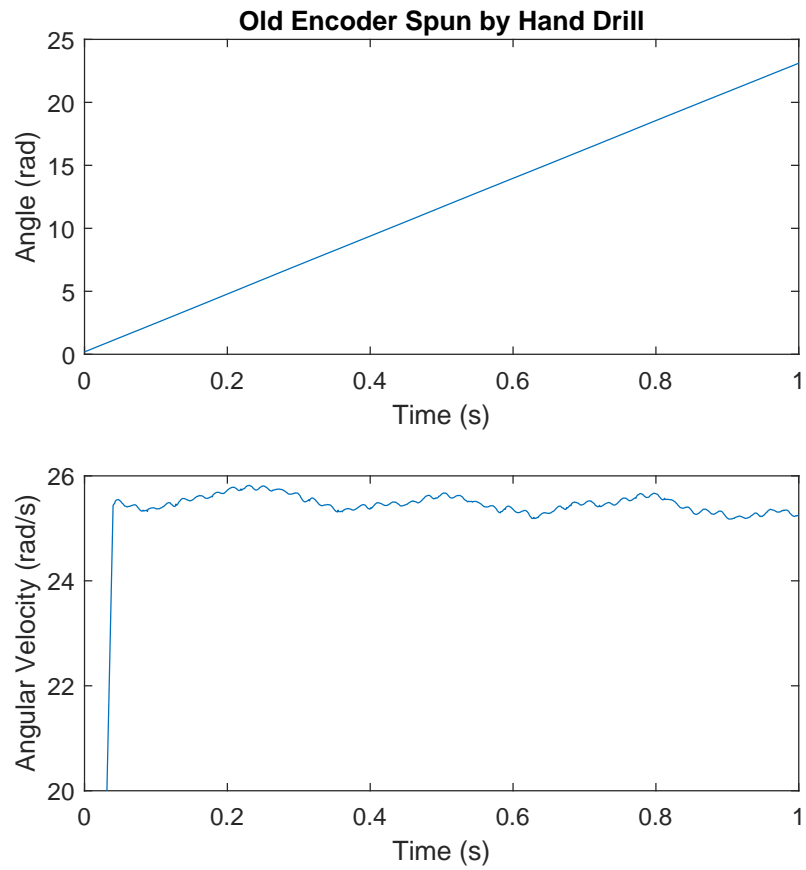


Figure 4-2: Old encoder (12-bit) data taken with hand drill test.

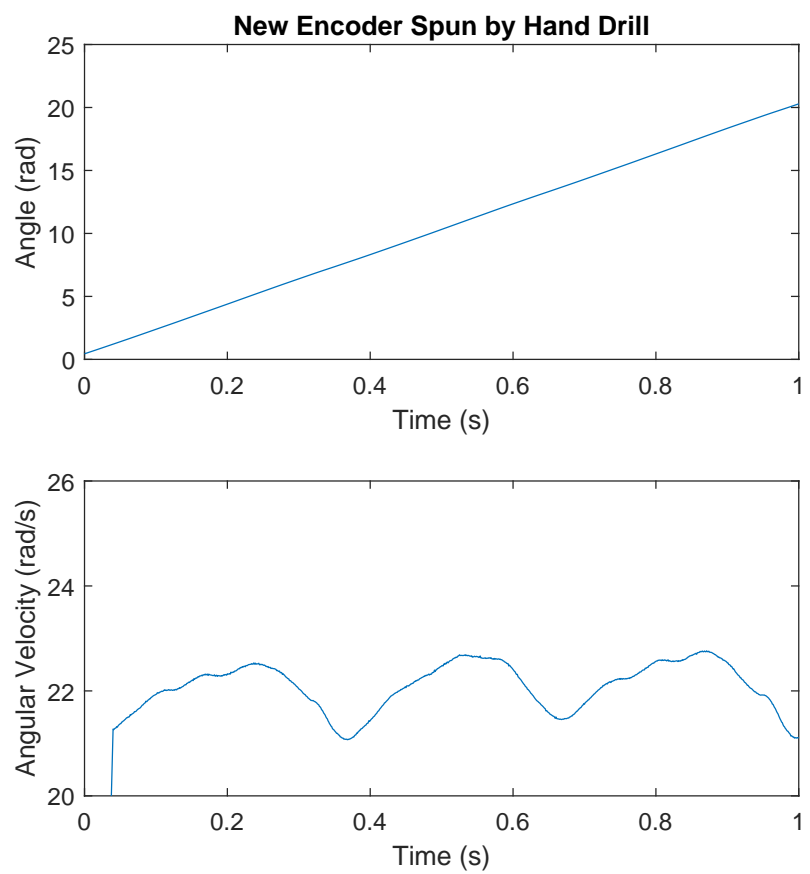


Figure 4-3: New encoder (19-bit) data taken with hand drill test.

The plot records position and velocity data from the microcontroller at 1 kHz. There is a noticeable high frequency ripple in the velocity data on the lower resolution encoder. There is also some lower frequency ripple seen on both, possibly due to the nature of the hand drill driving the module and so a new test was performed.

The next test for encoder data used the motor controller on the module to provide a constant velocity or position command. The same gains were used on both modules and so discrepancies in the plots are either due to noise or mechanical features.

Figure 4-4 and Figure 4-5 show the position and velocity data for the modules driving at constant velocity. The high frequency velocity ripple seen in the hand drill test with the low resolution encoder matches the high frequency velocity ripple seen in the driven motor controller data for the low resolution encoder.

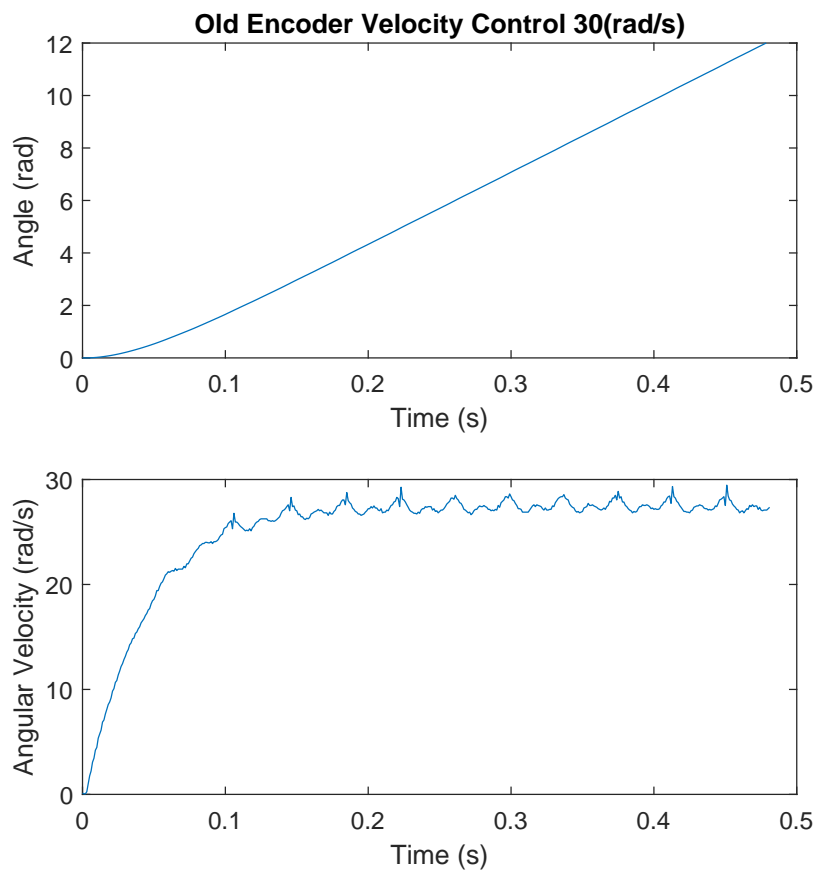


Figure 4-4: Old encoder (12-bit) data taken in constant velocity mode.

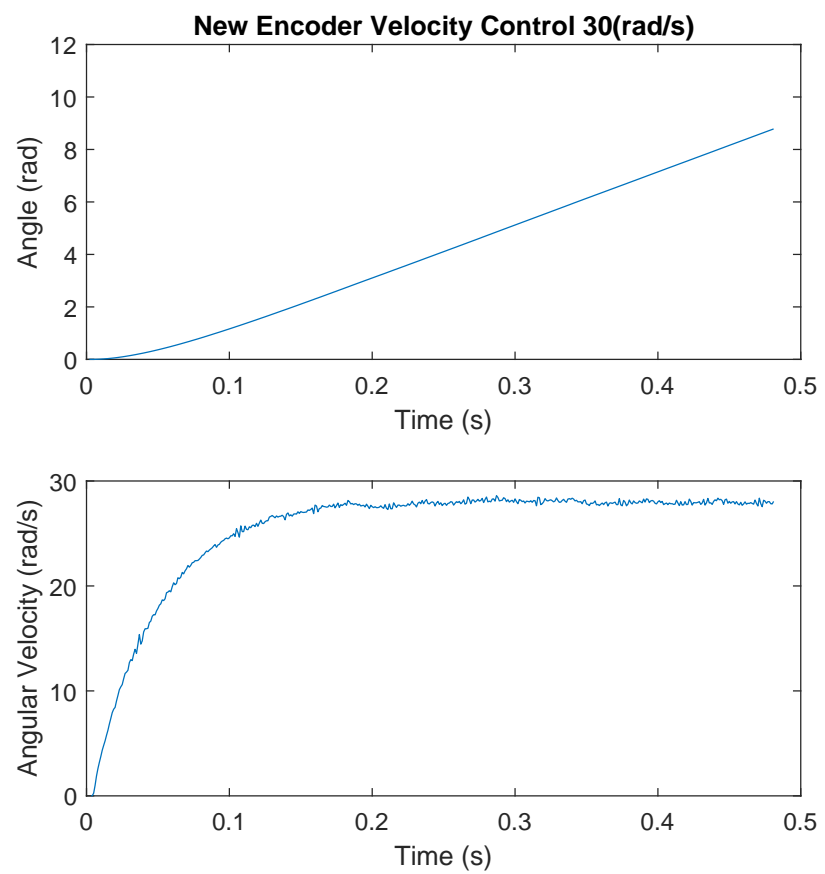


Figure 4-5: New encoder (19-bit) data taken in constant velocity mode.

There is a noticeable decrease in peak to peak velocity noise when switching to the high resolution encoder. The low resolution encoder data showed variations of up to 2 rad/s compared to 0.3 rad/s for the high resolution encoder. Additionally, the new encoder has built-in position data filtering which could be tested in the future.

A similar order of magnitude decrease in velocity noise was shown in tests at 0 velocity commanded, with the old encoder having velocity ripple with a peak to peak error of 0.4 rad/s and the new encoder showing a peak error of 0.04 rad/s. This is shown in Figure 4-6 and Figure 4-7.

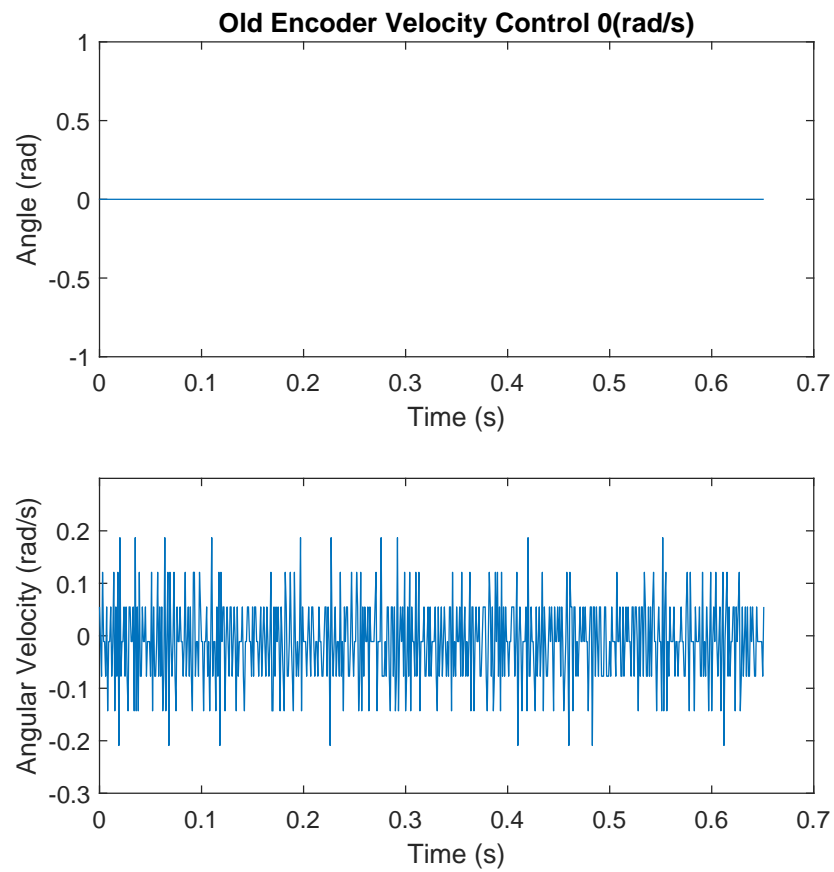


Figure 4-6: Old encoder (12-bit) data taken with 0 velocity commanded.

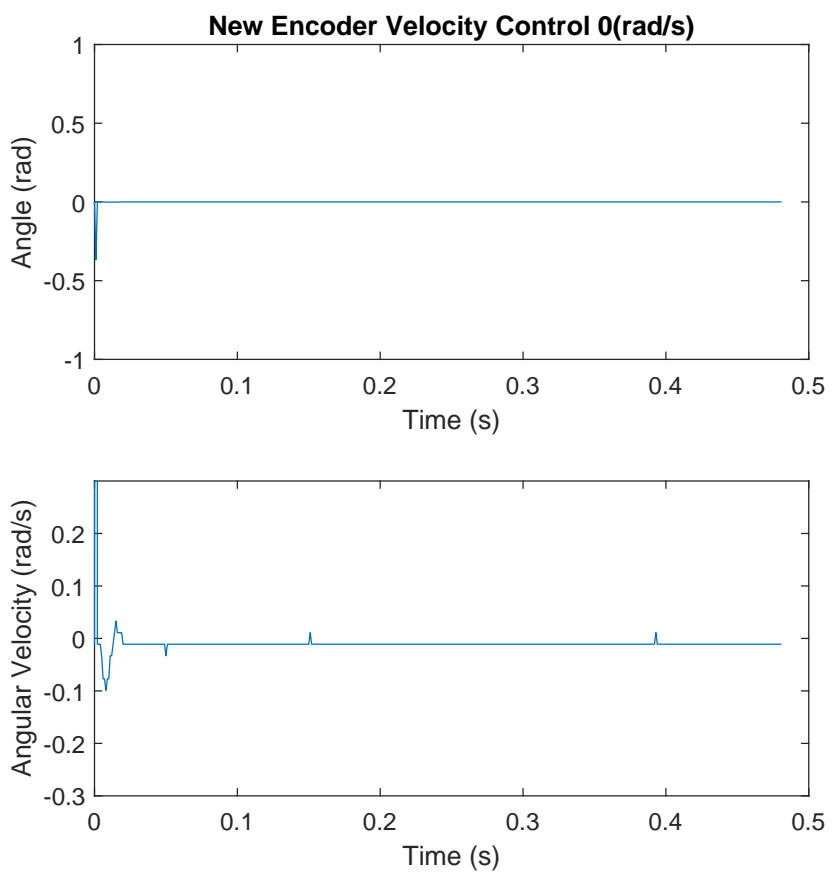


Figure 4-7: New encoder (19-bit) data taken with 0 velocity commanded.

One thing to note is that the position data for both encoders does have some noise but this is not captured in the data. This is because of the way the motor controller communicates over CAN. The motor controller uses 16 bits of data to represent the position of the output of the module (past the gearbox) between -4π and 4π so this binning of the output eliminates any noise on position when communicating over CAN. However, the same effect does not eliminate velocity noise (in particular, on the old encoder data) because it is still seen. Future tests could utilize new firmware that uses more bits of resolution for position and velocity data.

Additional plots of position and velocity data in a typical application are shown in Figure 4-8 and Figure 4-9.

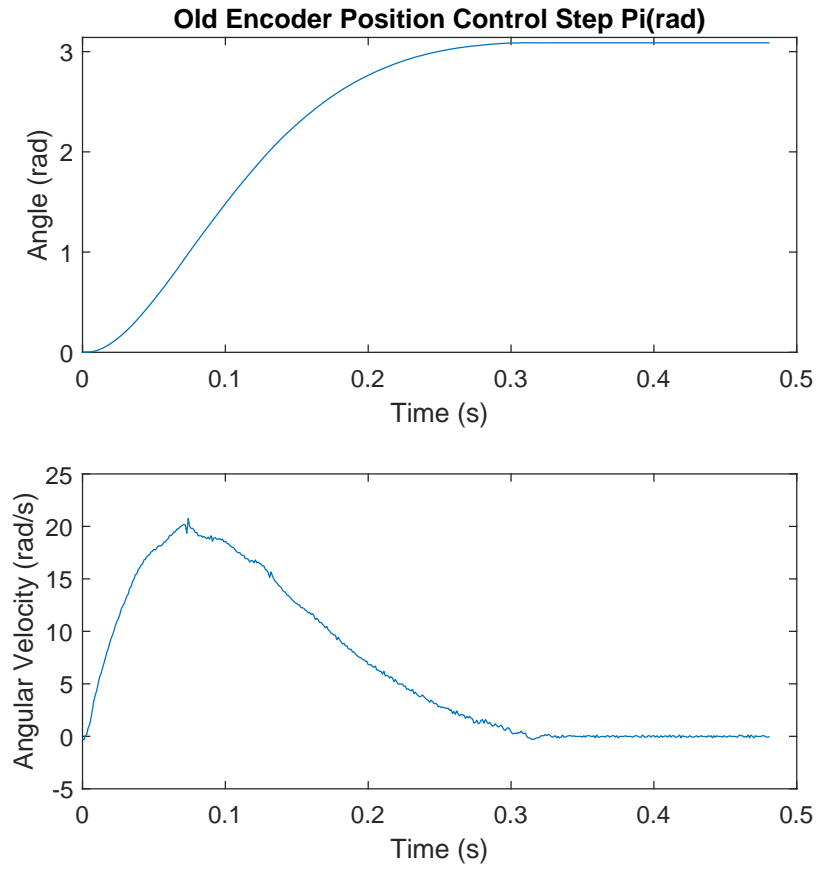


Figure 4-8: Old encoder (12-bit) data taken with a step response.

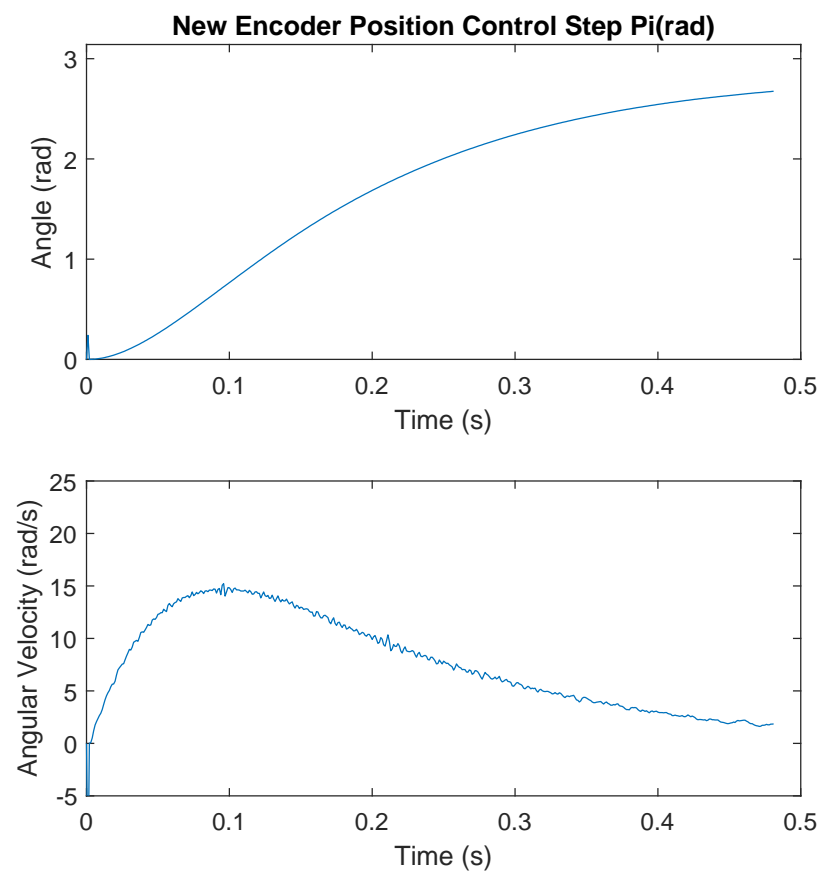


Figure 4-9: New encoder (19-bit) data taken with a step response.

4.3 Finite Element Analysis

As stated before, the alignment of the motor encoder magnet and the motor controller is important in order to have proper motor control. Finite element analysis (FEA) was done on the system to determine approximate magnet/encoder misalignment for appropriate loading cases, with the allowable misalignments taken from the IC datasheet. The actuator can be mounted in two ways; it can be mounted on the output side (front side) or on the back side. The mounting bolt locations are shown in Figure 4-10. It is recommended that the actuator is mounted on the output side in order to shorten the load path, but the worst case back side mounting was designed to be functional as well.

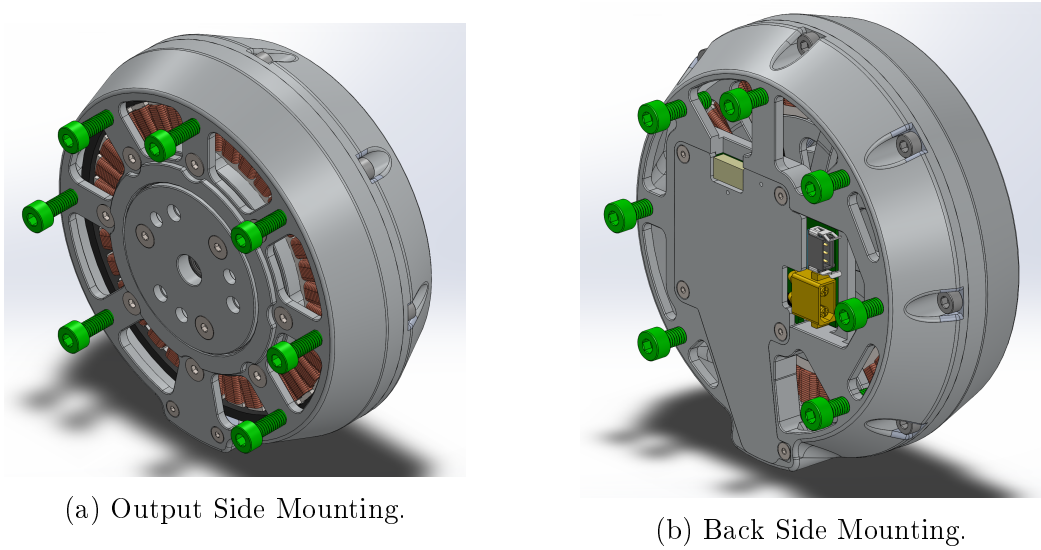
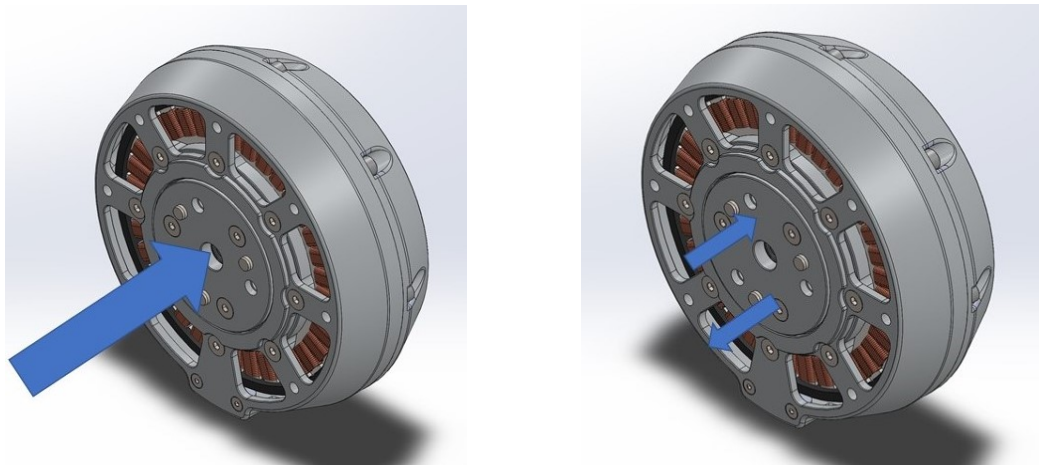


Figure 4-10: Bolts for mounting shown in green.

The maximum allowable radial and tangential displacement of the magnet and encoder from the nominal position is 0.5 mm in each direction. Therefore the maximum displacement of the location of the magnet is of interest. In order to decrease simulation complexity, the model was simplified by only using the critical components for analyzing the deformation. The crossed roller bearing is significantly stiffer than the machined pieces it is fixed to and so it was omitted for this simulation. Axial loading and torsional loading of the module when mounted from the output side and back side were analyzed. The loading conditions are shown in Figure 4-11.



(a) Axial loading of the actuator output. (b) Torsional loading of the actuator output.

Figure 4-11: Loading conditions of the actuator output simulated using FEA.

All simulations showed a max displacement of the module of less than .3 mm, with most being an order of magnitude or more below this. The worst case scenario of mounting from the back side and applying a torque was still within the acceptable range. Earlier FEA simulations were also used to aid in the design process by finding areas of unnecessary stiffness or lack thereof relative to one another. The results of some of the FEA simulations are shown in the following figures.

Figure 4-12 shows the module under axial loading when mounted in both mounting configurations (front or back). Although the rear mounting did show a greater overall max deflection, the greatest deflection seen at any point on the module in either mounting configuration was orders of magnitude less than the max overall allowable deflection of the magnet.

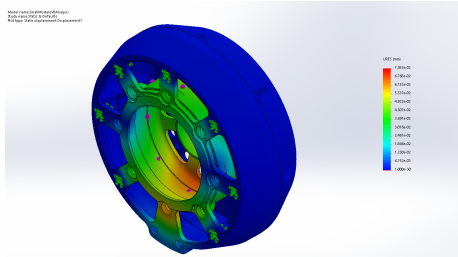


(a) Axial loading of the actuator output when mounted from the front.

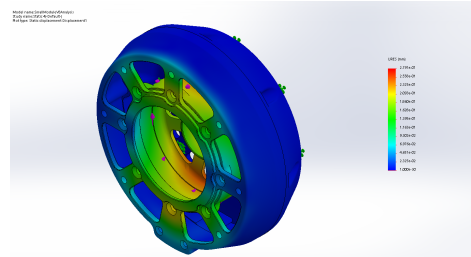
(b) Axial loading of the actuator output when mounted from the rear.

Figure 4-12: FEA of the module housing under axial loading.

Figure 4-13 shows the module under torsional loading when mounted in both mounting configurations. The closest the module got to deforming in a nonsignificant way was when torsionally loaded while mounted from the rear. However, the deflection was still in an acceptable range for the magnet.



(a) Torsional loading of the actuator output when mounted from the front.



(b) Torsional loading of the actuator output when mounted from the rear.

Figure 4-13: FEA of the module housing under torsional loading.

Chapter 5

Summary and Conclusions

5.1 Design Summary

This thesis documents the design and manufacturing of a high torque density robotic actuator consisting of a motor, gearbox, position sensor, and motor controller, in one housing. A prototype actuator module was developed in-house and the final design is being produced for use in humanoids, quadrupeds, and bilaterally teleoperated arms. The actuator builds on previous work by Ben Katz and Sangbae Kim who developed the original actuator modules for the Mini Cheetah robot. The new actuator uses a new mechanical topology, an improved mechanical design for the rotor, and a new encoder to improve overall performance while maintaining the same form factor with a small increase in weight.

Bibliography

- [1] iC Haus. *iC-MU MAGNETIC OFF-AXIS POSITION ENCODER*, 4 2020. Rev. E3.
- [2] iC Haus. *iC-MU MAGNETIC TARGET DESCRIPTION*, 4 2020. Rev. B1.
- [3] Ben Katz. A low cost modular actuator for dynamic robots. Master's thesis, MIT, Jun 2018.

